Planar nitrogen-doped aluminum clusters Al_xN^- ($x=3-5$)

Boris B. Averkiev and Alexander I. Boldyrev[a)]
Department of Chemistry and Biochemistry, Utah State University, 0300 Old Main Hill, Logan, Utah 84322-0300

Xi Li[b)] and Lai-Sheng Wang[c)]
Department of Physics, Washington State University, 2710 University Drive, Richland, Washington 99354 and Chemical Sciences Division, Pacific Northwest National Laboratory, MS K8-88, P.O. Box 999, Richland, Washington 99352

(Received 28 April 2006; accepted 14 July 2006; published online 22 September 2006)

The electronic and geometrical structures of three nitrogen-doped aluminum clusters, Al_xN^- ($x=3-5$), are investigated using photoelectron spectroscopy and *ab initio* calculations. Well-resolved photoelectron spectra have been obtained for the nitrogen-doped aluminum clusters at four photon energies (532, 355, 266, and 193 nm). Global minimum structure searches for Al_xN^- ($x=3-5$) and their corresponding neutrals are performed using several theoretical methods. Vertical electron detachment energies are calculated using three different methods for the lowest energy structures and low-lying isomers are compared with the experimental observations. Planar structures have been established for all the three Al_xN^- ($x=3-5$) anions from the joint experimental and theoretical studies. For Al_5N^-, a low-lying nonplanar isomer is also found to contribute to the experimental spectra, signifying the onset of two-dimensional to three-dimensional transition in nitrogen-doped aluminum clusters. The chemical bonding in all the planar clusters has been elucidated on the basis of molecular orbital and natural bond analyses. © *2006 American Institute of Physics*. [DOI: 10.1063/1.2335449]

I. INTRODUCTION

By doping pure metal clusters with one or more "impurity" atoms one can generate novel chemical species and manipulate their physical and chemical properties. Understanding how impurities affect the chemical bonding in doped clusters can provide valuable information in understanding nanomaterials and nanostructure interfaces and may be an important step in developing a robust chemical bonding model which could be used in the rational design of the smallest electronic devices based on nanoclusters. Aluminum is widely used as conductor in electronic devices and aluminum nitride (AlN) is an important semiconductor material. Several prior experimental and theoretical studies have been reported on small aluminum nitride Al_nN_m clusters.[1–11] In particular, Nayak *et al.* have reported a combined experimental and density functional study on Al_3N^- and Al_4N^-.[4] Recently, Li and Wang reported an extensive set of photoelectron spectra of Al_xN^- clusters from $x=2-22$ at 193 nm and compared them to those of pure Al_x^- clusters.[10]

The present contribution focuses on a detailed investigation of the electronic structure and chemical bonding in three small aluminum clusters doped with one impurity N atom, Al_xN^- and Al_xN^- ($x=3-5$). An extensive set of photoelectron spectra has been obtained for each anion at four detachment photon energies (532, 355, 266, and 193 nm). Well-resolved spectral features were interpreted using *ab initio* theoretical calculations at several levels of theory, which allow us to unequivocally elucidate the electronic and geometrical structures, stability, and low-lying isomers of these three anions and their corresponding neutrals. The ground states of all three species are found to be planar. Molecular orbital and natural bond analyses have been carried out to understand the chemical bonding in the planar clusters. We also found a nonplanar isomer of Al_5N^-, which is very close in energy to the planar ground state isomer and is present in the molecular beam, suggesting the onset of two-dimensional (2D) to three-dimensional (3D) structural transitions.

II. EXPERIMENTAL METHOD

The experiment was performed using a magnetic-bottle photoelectron spectroscopy (PES) apparatus with a laser vaporization cluster source. Details of this apparatus have been published elsewhere.[12] Briefly, the Al_xN^- clusters were produced by laser vaporization of either a pure Al or an AlN alloy disk target with a 5% N_2/He carrier gas. The anion clusters of interest were size selected and photoelectron spectra were taken at several different photon energies. The electron energy resolution was better than 30 meV for 1 eV electrons. We have measured photodetachment spectra of Al_xN^- for $x=2-45$ at 193 nm and reported those data up to $x=22$ recently.[10] In the current study, we obtained the photoelectron spectra of Al_xN^- with $x=3-5$ at four photon energies, 532 nm (2.331 eV), 355 nm (3.496 eV), 266 nm (4.661 eV), and 193 nm (6.424 eV), as shown in Figs. 1–3, respectively.

[a)]Electronic mail: boldyrev@cc.usu.edu
[b)]Present address: Rowland Institute at Harvard, Harvard University, 100 Edwin H. Land Blvd., Cambridge, MA 02142.
[c)]Electronic mail: ls.wang@pnl.gov

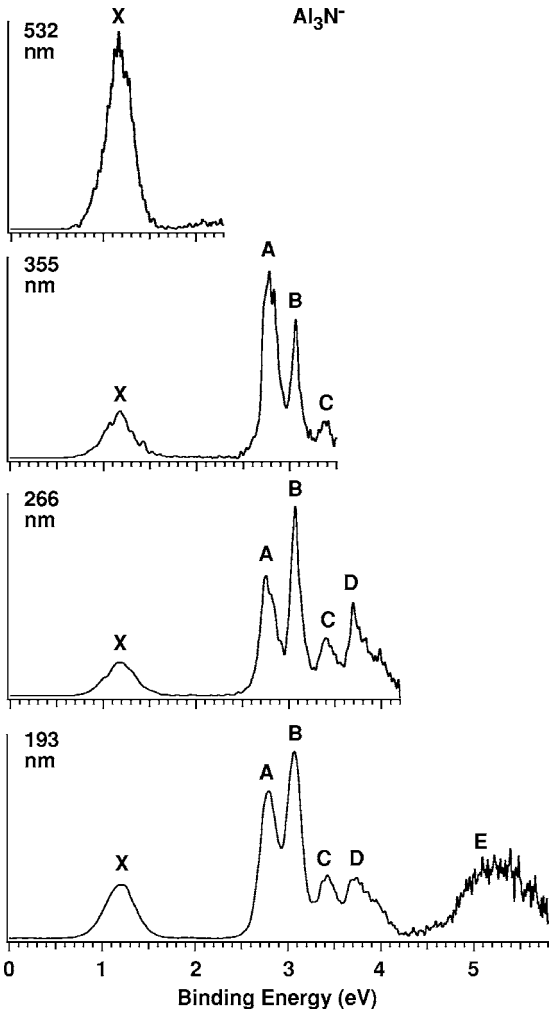

FIG. 1. Photoelectron spectra of Al_3N^- at four photon energies: 532 nm (2.331 eV), 355 nm (3.496 eV), 266 nm (4.661 eV), and 193 nm (6.424 eV).

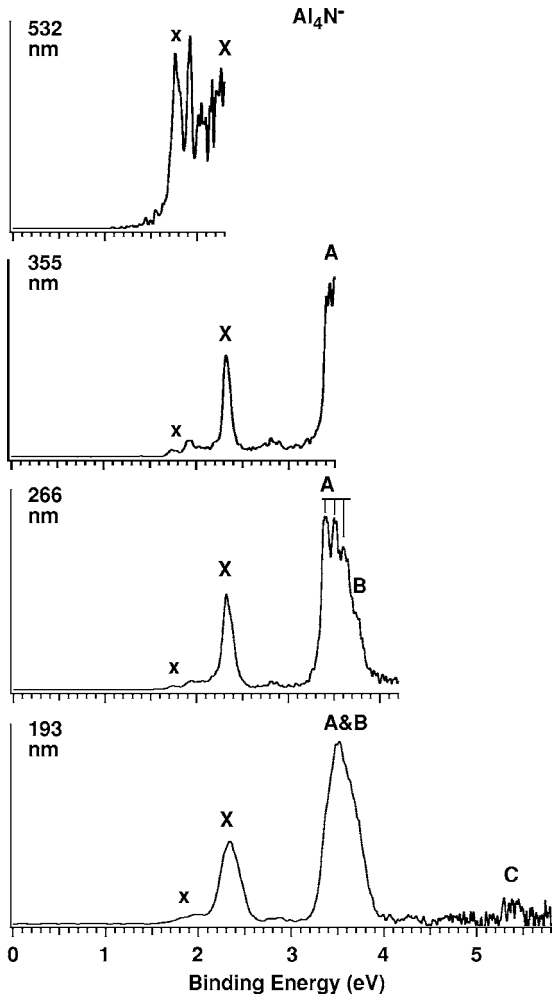

FIG. 2. Photoelectron spectra of Al_4N^- at four photon energies: 532 nm (2.331 eV), 355 nm (3.496 eV), 266 nm (4.661 eV), and 193 nm (6.424 eV).

III. THEORETICAL METHODS

The initial search for the most stable structures was performed using our gradient embedded genetic algorithm (GEGA) program written by Alexandrova.[13,14] We used a hybrid method known in the literature[15–17] as B3LYP with the small split-valence basis sets[18] (3-21G) for energy, gradient, and force calculations. The lowest few structures in every system were recalculated using the B3LYP, a second order Moller-Plesset perturbation theory (MP2),[19] and coupled-cluster method with single, double, and noniterative triple excitations[20–22] [CCSD(T)] based on the unrestricted Hartree-Fock (UHF) formalism for open-shell systems and all with the polarized split-valence basis sets (6-311+G*).[23–25] Total energies of these structures were also calculated using the extended 6-311+G(2*df*) basis sets. In order to test the validity of the one-electron approximation, single point calculations were performed using the multiconfiguration self-consistent-field method[26,27] [CASSCF(X,Y)] with X active electrons and Y active molecular orbitals.

The vertical electron detachment energies were calculated using R(U)CCSD(T)/6-311+G(2*df*) and the outer valence Green's function method[28–32] [R(U)OVGF/6-311+G(2*df*)] at the CCSD(T)/6-311+G* geometries, as well as at the time-dependent density-functional theory (DFT) method[33,34] [TD-B3LYP/6-311+G(2*df*)] at the B3LYP/6-311+G* geometries. Core electrons were frozen in treating the electron correlation at the R(U)CCSD(T) and R(U)OVGF levels of theory.

The B3LYP, MP2, R(U)CCSD(T), and R(U)OVGF *ab initio* calculations were performed using the GAUSSIAN 98 and GAUSSIAN 03 programs.[35,36] Molecular orbital visualization has been done using the MOLDEN3.4 program.[37]

IV. EXPERIMENTAL RESULTS

The 193 nm spectrum of Al_3N^- (Fig. 1) reveals six spectral bands below 5.8 eV, labeled as X, A, B, C, D, and E, respectively. The features X (around 1.19 eV) and E (around 5.2 eV) are very broad. The onset of the first two transitions at 1.19 and 2.78 eV represents a large energy gap, suggesting that the neutral Al_3N cluster is likely to be closed shell with a large highest occupied molecular orbital (HOMO)-lowest unoccupied molecular orbital (LUMO) gap. The broad nature of the X band indicates that there is a significant geometry change between the ground states of the anion and neutral.

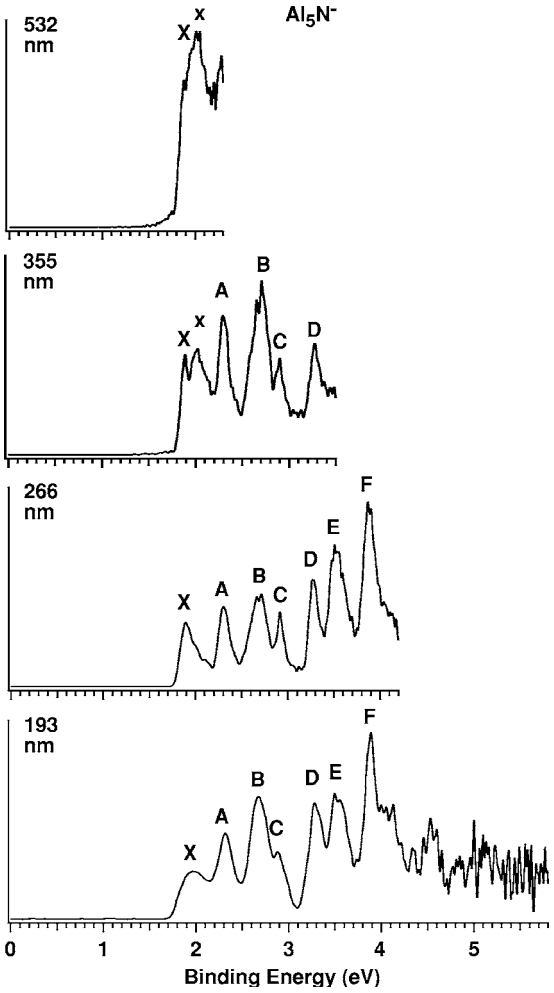

FIG. 3. Photoelectron spectra of Al_5N^- at four photon energies: 532 nm (2.331 eV), 355 nm (3.496 eV), 266 nm (4.661 eV), and 193 nm (6.424 eV).

The spectral features are better resolved in the lower photon energy spectra and the obtained vertical detachment energies (VDEs) are given in Table I.

The spectra of Al_4N^- (Fig. 2) are surprisingly simple with only two intense bands observed in the 193 nm spectrum. The X band at 2.32 eV in the 355 and 266 nm spectra is very sharp with no indication of any vibrational structure, whereas the 3.41 eV feature (A) is broad with a partially resolved vibrational progression, which yields a vibrational frequency of 810 ± 50 cm^{-1}. A shoulder on the higher binding energy side of the A band is identified as another electronic transition, labeled as B. A weak band (C) is observed in the 193 nm at very high binding energies. There are also other weak features present in the spectra of Al_4N^-. The features, occurring at around 1.76(x) and 1.93 eV, are resolved more clearly at lower photon energies, especially at 532 nm. There are also weak signals around 2.7 eV. The intensities of these features depend on the source conditions slightly but could not be eliminated. All these weak features are most likely due to excited states or different isomers of Al_4N^-.

The spectra of Al_5N^- are quite complicated with numerous well-defined features (X, A, B, C, D, E, and F) at 266 nm (Fig. 3), and more features are also revealed at higher binding energies in 193 nm. A strong feature around 2.01 eV (x) at both 532 and 355 nm is resolved, which appears to be merged with the X band. The complicated spectra of Al_5N^- suggest the possible population of closely lying isomers, as born out from our theoretical calculations.

The VDEs of the main spectral features for Al_xN^- ($x=3$, 4, and 5) are all given in Table I and are compared with *ab initio* results in Tables V–VII, respectively (*vide infra*).

V. THEORETICAL RESULTS

We performed extensive searches for the global minimum structures of Al_xN^- ($x=3-5$) and their neutrals using our GEGA program at the B3LYP/3-21G level of theory.

A. Al_3N and Al_3N^-

The planar $D_{3h}(^1A_1', 1a_1'^2 1e'^4 2a_2''^2 2a_1'^2 2e'^4 3e'^0)$ structure I (Fig. 4) was found to be the global minimum structure for Al_3N from prior *ab initio* calculations[3–6] and from infrared matrix investigations.[6] Andrews *et al.* assigned two sharp bands at 777.9 and 770.3 cm^{-1} to the e' antisymmetric stretching mode of Al_3N split by interaction in nitrogen matrix. The major peak at 773.1 cm^{-1} in argon matrix was assigned to the same mode. Our calculations of the planar $D_{3h}(^1A_1')$ geometric structure for Al_3N (Table II) at our highest level of theory [CCSD(T)/6-311+G*] reveal $\omega_3(e')=776$ cm^{-1}, in excellent agreement with the matrix experiment.

For the Al_3N^- anion we performed GEGA search at the B3LYP/3-21G level of theory. The two lowest (below 20 kcal/mol) doublet structures are presented in Figure 4. The planar T-shaped $C_{2v}(^2B_2, 1a_1^2 1b_2^2 2a_1^2 1b_1^2 3a_1^2 2b_2^2 4a_1^2 3b_2^1)$ structure II is predicted by GEGA to be the global minimum structure, similar to that reported previously by Nayak *et al.*[4] using DFT calculations. The second $C_{2v}(^2A_1)$ configuration originated from the $1a_1'^2 1e'^4 2a_2''^2 2a_1'^2 2e'^4 3e'^1$ occupation is a first order saddle point on the intramolecular rearrangement of the anion from one global minimum structure into another. We performed single point calculations at the CASSCF(7,8)/6-311+G*, CASSCF(7,10)/6-311+G*, and CASSCF(13,12)/6-311+G* and found that the Hartree-Fock wave function was dominant ($C_{HF}=0.949$, $C_{HF}=0.943$,

TABLE I. Experimental vertical detachment energies in eV for the Al_3N^-, Al_4N^-, and Al_5N^- anions from the photoelectron spectra. The number in parentheses represents the uncertainty of the last digit.

	X	A	B	C	D	E	F
Al_3N^-	1.19(4)	2.78(3)	3.06(3)	3.39(4)	3.69(4)	5.20(5)	
Al_4N^-	2.32(3)	3.41(2)	3.7(1)	5.40(5)			
Al_5N^-	1.89(4)	2.29(3)	2.66(3)	2.90(3)	3.27(3)	3.51(3)	3.87(3)

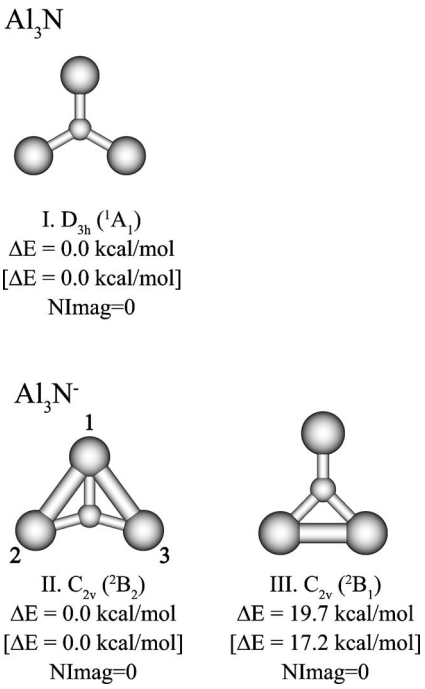

FIG. 4. The lowest isomers for Al_3N and Al_3N^-. Relative energies are presented at CCSD(T)/6-311+G(2*df*)//B3LYP/6-311+G* and at B3LYP/6-311+G* in brackets. N_{imag} is the number of imaginary frequencies calculated at B3LYP/6-311+G*.

and $C_{HF}=0.945$, respectively) in the CASSCF expansion, thus confirming the applicability of MP2 and CCSD(T) theoretical methods. However, at our highest level of theory [CCSD(T)/6-311+G*] the planar T-shaped $C_{2v}(^2B_2)$ structure is a saddle point with the $\omega_3(b_1)=37i$ cm^{-1} imaginary frequency (Table II). Geometry optimization following the imaginary frequency leads to a slightly nonplanar structure $C_s(^2A'')$ with the nitrogen atom being out of plane by 0.04 Å. The energy difference between the planar and nonplanar structures is only 5.6×10^{-4} kcal/mol and that value is significantly lower than the difference in zero point energy (ZPE) corrections (0.065 kcal/mol) for the two structures. Thus, the vibrationally averaged Al_3N^- structure is actually planar and for all practical purpose we will consider Al_3N^- as being planar in the following discussion. The lowest alternative structure III $(C_{2v},{}^2B_1,1a_1^22a_1^21b_2^21b_1^23a_1^22b_2^24a_1^22b_1^1)$ corresponds to a local minimum, which is substantially higher in energy and will not be further discussed.

The T shape for the isoelectronic Al_3O cluster was predicted before by Boldyrev and Schleyer[38] and Sun *et al.*[39] with quite similar molecular parameters. The $CAlSi_2$ cluster, another 15 valence electron tetra-atomic molecule, was, however, found to have a Y-type structure by Boldyrev *et al.*[40] When an additional electron is added to Al_3N^-, the resulting 16 valence electronic Al_3N^{2-} cluster was found to have the T shape again, which has been found to be the ground state for all other studied isoelectronic species such as BSi_3^-, $CAlSi_2^-$, CSi_3, NSi_3^+, NAl_2Si^-, Al_3O^-, and Al_3F.[40]

B. Al_4N and Al_4N^-

For Al_4N the GEGA search led to a global minimum planar $D_{4h}(^2B_{2g},1a_{1g}^21e_u^41a_{2u}^22a_{1g}^21b_{1g}^22e_u^41b_{2g}^1)$ structure IV (Fig. 5), in agreement with several previously reported theoretical studies.[3–5,7,9] At our highest level of theory

TABLE II. The molecular properties of the global minimum Al_3N^- and Al_3N structures.

Molecular parameter	Al_3N^- $(C_{2v},{}^2B_2')$ B3LYP/6-311+G*	Al_3N^- $(C_{2v},{}^2B_2')$ MP2/6-311+G*	Al_3N^- $(C_{2v},{}^2B_2')$ CCSD(T)/6-311+G*	Al_3N^- $(C_s,{}^2A'')$ CCSD(T)/6-311+G*[a]
E(a.u.)	−782.2040	−780.6194	−780.667 437 6	−780.667 438 5[b]
R(N−Al_1)(Å)	1.916	1.923	9.916	1.916
R(N−$Al_{2,3}$)(Å)	1.822	1.827	1.821	1.821
∠$Al_1NAl_{2,3}$(deg)	102.9	101.8	102.4	102.4
$\omega_1(a_1)$(cm^{-1})	560 (80.2)[c]	569 (101.5)[c]	577	577
$\omega_2(a_1)$(cm^{-1})	444 (0.6)[c]	445 (1.0)[c]	452	452
$\omega_3(a_1)$(cm^{-1})	152 (8.3)[c]	156 (12.2)[c]	153	153
$\omega_3(b_1)$(cm^{-1})	164 (4.1)[c]	57 (2.9)[c]	37*i*	46
$\omega_4(b_2)$(cm^{-1})	801 (4.7)[c]	822 (1.2)[c]	822	821
$\omega_4(b_2)$(cm^{-1})	140 (22.8)[c]	175 (27.9)[c]	136	137

Molecular parameter	Al_3N $(D_{3h},{}^1A_1')$ B3LYP/6-311+G*	Al_3N $(D_{3h},{}^1A_1')$ MP2/6-311+G*	Al_3N $(D_{3h},{}^1A_1')$ CCSD(T)/6-311+G*
E(a.u.)	−782.1750	−780.6034	−780.6512
R(N−Al)(Å)	1.850	1.851	1.847
$\omega_1(a_1')$(cm^{-1})	426 (0.0)[a]	428 (0.0)[c]	438
$\omega_2(a_2'')$(cm^{-1})	218 (0.1)[c]	133 (0.0)[c]	137
$\omega_3(e')$(cm^{-1})	749 (328.1)[c]	765 (334.7)[c]	776
$\omega_4(e')$(cm^{-1})	154 (2.8)[c]	150 (3.2)[c]	151

[a]$E_{tot}=-780.735\,852$ a.u..
[b]$E_{tot}=-780.709\,937$ a.u. [all at CCSD(T)/6-311+G(2*df*)//CCSD(T)/6-311+G*]. Nitrogen atom comes out of the Al_3 plane by 0.039 Å.
[c]Values in parentheses represent relative absorbance intensities in the IR spectrum.

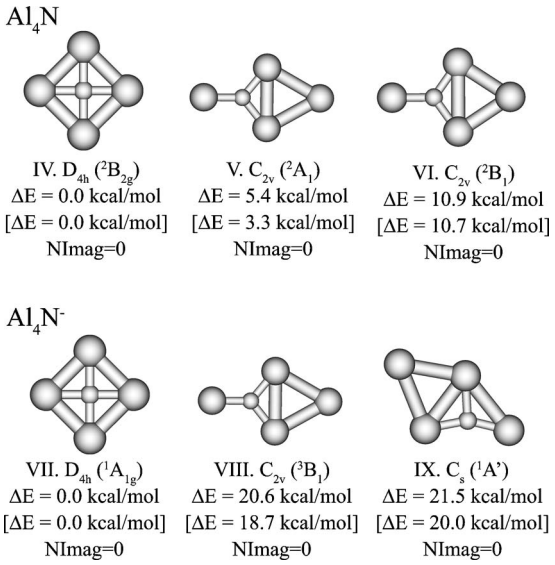

FIG. 5. The lowest isomers for Al_4N and Al_4N^-. Relative energies are presented at CCSD(T)/6-311+G(2*df*)//B3LYP/6-311+G* and at B3LYP/6-311+G* in brackets. N_{imag} is the number of imaginary frequencies calculated at B3LYP/6-311+G*.

CCSD(T)/6-311+G*, the $D_{4h}(^2B_{2g})$ structure is a saddle point (Table III). Distortion along the b_{2u} mode of imaginary frequency leads to a slightly nonplanar butterfly distorted structure $D_{2d}(^2B_1)$. However, the energy difference between $D_{2d}(^2B_1)$ and $D_{4h}(^2B_{2g})$ is only 0.192 kcal/mol, which is smaller than the difference in ZPE (0.206 kcal/mol). Therefore, the vibrationally averaged structure is actually planar and in the following discussion we will consider the Al_4N cluster to be planar. The similar small deviation from planarity was previously reported for the valence isoelectronic Al_4C^- anion.[41] The planar structure was also found to be a global minimum structure for other 18 valence electron penta-atomic species Al_4O,[1,38,39] Al_2Si_2C,[1,42] Al_2Ge_2C,[1,42] Al_3SiC^-,[43] and Al_3GeC^-,[43] as well as for other 17 valence electron penta-atomic species Al_4C^-,[41] Al_3SiC,[43] and Al_3GeC.[43] Hence, the 18 and 17 electron rule[1,38,42–45] for planarity of penta-atomic clusters is a general rule for these species.

For the neutral Al_4N cluster, in addition to the global minimum $D_{4h}(^2B_{2g})$ structure IV, we also found two low-lying isomers $C_{2v}(^2A_1)$ (structure V in Fig. 5) and $C_{2v}(^2B_1)$ (structure VI in Fig. 5), which are 5.4 and 10.9 kcal/mol above the global minimum at the CCSD(T)/6-311+G(2*df*)//B3LYP/6-311+G* level of theory.

The planar $D_{4h}(^1A_{1g})$ structure for Al_4N^- was first computationally predicted by Schleyer and Boldyrev[1] on the basis of molecular orbital analysis for the five-atomic 18 valence electron systems and was confirmed in follow up calculations.[2,4,5,7] In order to confirm these results for the Al_4N^- anion, we run GEGA calculations for both singlet and triplet states of the Al_4N^- anion. The lowest (less than about 20 kcal/mol) singlet and triplet structures found by GEGA are presented in Fig. 5. The GEGA search found the planar $D_{4h}(^1A_{1g}, 1a_{1g}^2 1e_u^4 1a_{2u}^2 2a_{1g}^2 1b_{1g}^2 2e_u^4 1b_{2g}^2)$ structure VII to be the global minimum, in agreement with previously reported theoretical results.[1,2,4,5,7] We performed single point calculations at the CASSCF(8,8)/6-311+G*, CASSCF(12,12)/6-311+G*, and CASSCF(8,14)/6-311+G* and found that the Hartree-Fock wave function was dominant (C_{HF}=0.980, C_{HF}=0.969, and C_{HF}=0.958, respectively) in the CASSCF expansion. We found that the next lowest isomer is a triplet $C_{2v}(^3B_1, 1a_1^2 2a_1^2 1b_2^2 3a_1^2 1b_1^2 4a_1^2 2b_2^2 5a_1^2 6a_1^1 2b_1^1)$ structure VIII [20.6 kcal/mol higher at CCSD(T)/6-311+G(2*df*)//B3LYP/6-311+G*], which is similar to previously reported triplet structure by Nayak *et al.*[4] using DFT calculations, though they did not specify the spectroscopic state of their triplet isomer. We also found one singlet structure IX (C_s, $^1A'$, $1a'^2 2a'^2 3a'^2 4a'^2 1a''^2 5a'^2 6a'^2 7a'^2 8a'^2$), which is more than 20 kcal/mol higher.

C. Al_5N and Al_5N^-

For Al_5N the GEGA (B3LYP/3-21G) search found many structures (Fig. 6, X–XXI) with the planar $C_{2v}(^1A_1, 1a_1^2 2a_1^2 1b_2^2 3a_1^2 1b_1^2 4a_1^2 2b_2^2 3b_2^2 5a_1^2 6a_1^2)$ structure being the global minimum. The refinement at B3LYP/6-311+G* and at CCSD(T)/6-311+G(2*df*)//B3LYP/6-311+G* confirmed our GEGA results. However, at MP2/6-311+G* and CCSD(T)/6-311+G*, it has one imaginary frequency (Table IV). The most stable structure $C_s(^1A')$ at the last two levels of theory is only slightly distorted from the C_{2v} symmetry and after ZPE corrections it is effectively C_{2v} symmetry. The $C_{2v}(^1A_1)$ structure X was also reported to be the global minimum structure by Guo and Wu[9] who used two B3LYP/6-311+G* and SVWN/6-311+G* theoretical methods. According to Ling *et al.*[8] the global minimum of Al_5N corresponds to the structure XVIII at the full-potential linear-muffin-tin-orbital molecular dynamics (FP-LMTO-MD) method. We found that this structure is a second order saddle point, which is 17.3 kcal/mol higher in energy at B3LYP/6-311+G* [13.5 kcal/mol at CCSD(T)/6-311+G(2*df*)//B3LYP/6-311+G*]. Geometry optimization of the structure XVIII following the imaginary frequency led initially to the structure XII, and geometry optimization following the imaginary in the structure XII led eventually to the global minimum structure X. Thus, the structure XVIII can be safely excluded from being a global minimum structure of Al_5N. Nayak *et al.*[3] reported that the structure XI is the global minimum structure for the Al_5N cluster using the BPW91/6-311G** level of theory. The same global minimum structure was also reported by Leskiw *et al.*[7] According to our calculations, the structure XI is a first order saddle point at B3LYP/6-311+G*. Geometry optimization of the structure XI following the imaginary frequency led to a slightly distorted structure $C_2(^1A)$ in which the top Al atom still located on the C_2 axis with the beneath tetrahedral-type Al_4 cluster being slightly distorted. The energy difference between the $C_{2v}(^1A_1)$ structure XI and slightly distorted local minimum structure is only 0.021 kcal/mol, which is significantly lower than the difference in ZPE corrections (0.063 kcal/mol) for the two structures. At the MP2/6-311+G* and CCSD(T)/6-311+G* levels of theory, the $C_{2v}(^1A_1)$ structure was found to be a minimum. Thus, for all practical purpose, we will consider the structure XI of Al_5N as being C_{2v} symmetry. The structure XI is 6.8 kcal/mol higher in

TABLE III. The molecular properties of the Al_4N^- and Al_4N species. Values in parentheses represent relative absorbance intensities in the IR spectrum (km/mol).

Molecular parameter	Al_4N^- (D_{4h},$^1A_1$)			Al_4N (D_{4h},$^2B_{2g}$)			Al_4N (D_{2d},$^2B_1$)
	B3LYP/6-311+G*	MP2/6-311+G*	CCSD(T)/6-311+G*[a]	B3LYP/6-311+G*	MP2/6-311+G*	CCSD(T)/6-311+G*[b]	CCSD(T)/6-311+G*[b]
E(a.u.)	−1024.6857	−1022.6343	−1022.6869	−1024.6060	−1022.5538	−1022.6130	−1022.6133
R(N–Al)(Å)	1.936	1.938	1.936	1.964	1.968	1.962	1.961
$\omega_1(a_{1g})$(cm^{-1})	400 (0.0)	403 (0.0)	407	379 (0.0)	381 (0.0)	387	386
$\omega_2(a_{2u})$(cm^{-1})	214 (14.1)	118 (15.5)	117	223 (5.6)	159 (8.5)	151	220
$\omega_3(b_{1g})$(cm^{-1})	265 (0.0)	280 (0.0)	277	216 (0.0)	231 (0.0)	232	236
$\omega_4(b_{2g})$(cm^{-1})	268 (0.0)	278 (0.0)	275	223 (0.0)	244 (0.0)	245	265
$\omega_5(b_{2u})$(cm^{-1})	90 (0.0)	71 (0.0)	55	46 (0.0)	52 (0.0)	46*i*	47
$\omega_6(e_u)$(cm^{-1})	666 (238.8)	709 (345.2)	680	521 (123.5)	711 (505.5)	554	555
$\omega_7(e_u)$(cm^{-1})	217 (14.9)	251 (17.4)	226	97 (0.2)	316 (0.2)	159	160

[a] E_{tot}=−1022.770 084 a.u.
[b] E_{tot}=−1022.686 211 a.u. [all at CCSD(T)/6-311+G(2*df*)//CCSD(T)/6-311+G*].

energy than the structure X at B3LYP/6-311+G*, but this difference is only 1.3 kcal/mol at CCSD(T)/6-311+G(2*df*)//B3LYP/6-311+G* and 1.3 kcal/mol at CCSD(T)/6-311+G(2*df*)//CCSD(T)/6-311+G*. Thus, these two structures are almost degenerate at our highest level of theory. Two structures (XIV and XVI) were found to have two and one imaginary frequencies at B3LYP/6-311+G* level of theory: however, they have effective C_{2v} symmetry after ZPE corrections. Other structures identified in our calculations, within 20 kcal/mol above the ground state, are summarized in Fig. 6.

The structure of the Al_5N^- anion has been previously studied by Leskiw *et al.*,[7] who reported that the global minimum structure XXIII is similar to the structure XI for Al_5N neutral. Our GEGA search at B3LYP/3-21G for Al_5N^- found the planar $C_{2v}(^2B_1, 1a_1^2 2a_1^2 1b_2^2 3a_1^2 1b_1^2 4a_1^2 2b_2^2 3b_2^2 5a_1^2 6a_1^2 2b_1^1)$ structure XXII to be the global minimum, which is similar to the global minimum of the neutral (structure X). We also performed single point calculations at CASSCF(13,11)/6-311+G*, CASSCF(11,11)/6-311+G*, and CASSCF(11,12)/6-311+G* and found that the Hartree-Fock wave function was dominant (C_{HF}=0.932, C_{HF}=0.925, and C_{HF}=0.912, respectively) in the CASSCF expansion. At MP2/6-311+G* and CCSD(T)/6-311+G* it has one and two imaginary frequencies, respectively (Table IV). However, the vibrationally averaged global minimum structure can be considered to have the C_{2v} symmetry. The second lowest energy structure $C_s(^2A')$ in our calculations at B3LYP/3-21G, B3LYP/6-311+G*, and MP2/6-311+G* is similar to the global minimum structure XXIII proposed by Leskiw *et al.*,[7] though in our case it has lower symmetry C_s

TABLE IV. The molecular properties of the Al_5N^- and Al_5N species.

Molecular parameter	Al_5N^- (C_{2v},$^2B_1$)			Al_5N (C_{2v},$^1A_1$)		
	B3LYP/6-311+G*	MP2/6-311+G*	CCSD(T)/6-311+G*[a]	B3LYP/6-311+G*	MP2/6-311+G*	CCSD(T)/6-311+G*[b]
E(a.u.)	−1267.1276	−1264.5970	−1264.6622	−1267.0636	−1264.5370	−1264.6025
R(N–Al$_1$)(Å)	3.859	3.796	3.847	3.885	3.858	3.878
R(N–Al$_{2,3}$)(Å)	1.934	1.929	1.940	1.890	1.888	1.896
R(N–Al$_{4,5}$)(Å)	1.921	1.932	1.915	9.975	1.977	1.971
∠Al$_1$NAl$_{2,3}$(deg)	42.7	42.8	42.2	46.9	46.9	46.2
∠Al$_1$NAl$_{4,4}$(deg)	134.3	135.7	133.5	136.3	136.4	135.8
$\omega_1(a_1)$(cm^{-1})	666 (311)[c]	806 (1237)	707	697 (271)[c]	738 (356)	707
$\omega_2(a_1)$(cm^{-1})	411 (6)[c]	493 (28)	418	402 (32)[c]	407 (29)	408
$\omega_3(a_1)$(cm^{-1})	304 (1)[c]	353 (0)	327	284 (14)[c]	297 (18)	297
$\omega_4(a_1)$(cm^{-1})	243 (19)[c]	295 (6)	251	238 (3)[c]	256 (4)	242
$\omega_5(a_1)$(cm^{-1})	211 (4)[c]	246 (18)	224	196 (37)[c]	206 (51)	204
$\omega_6(a_1)$(cm^{-1})	67 (0)[c]	7 (0)	43*i*	82 (0)[c]	65 (0)	38
$\omega_7(b_1)$(cm^{-1})	213 (5)[c]	46 (0)	28	200 (2)[c]	10 (0)	72
$\omega_8(b_1)$(cm^{-1})	29 (2)[c]	78*i* (9)	62*i*	34 (3)[c]	31*i* (5)	32*i*
$\omega_9(b_2)$(cm^{-1})	628 (67)[c]	660 (64)	642	655 (110)[c]	717 (160)	663
$\omega_{10}(b_2)$(cm^{-1})	262 (3)[c]	284 (5)	268	246 (6)[c]	281 (7)	261
$\omega_{11}(b_2)$(cm^{-1})	209 (8)[c]	239 (7)	220	226 (1)[c]	256 (1)	234
$\omega_{12}(b_2)$(cm^{-1})	115 (0)[c]	166 (3)	117	106 (3)[c]	122 (3)	109

[a] E_{tot}=−a.u.
[b] E_{tot}=−a.u. [all at CCSD(T)/6-311+G(2*df*)//CCSD(T)/6-311+G*].
[c] Values in parentheses represent relative absorbance intensities in the IR spectrum (km/mol).

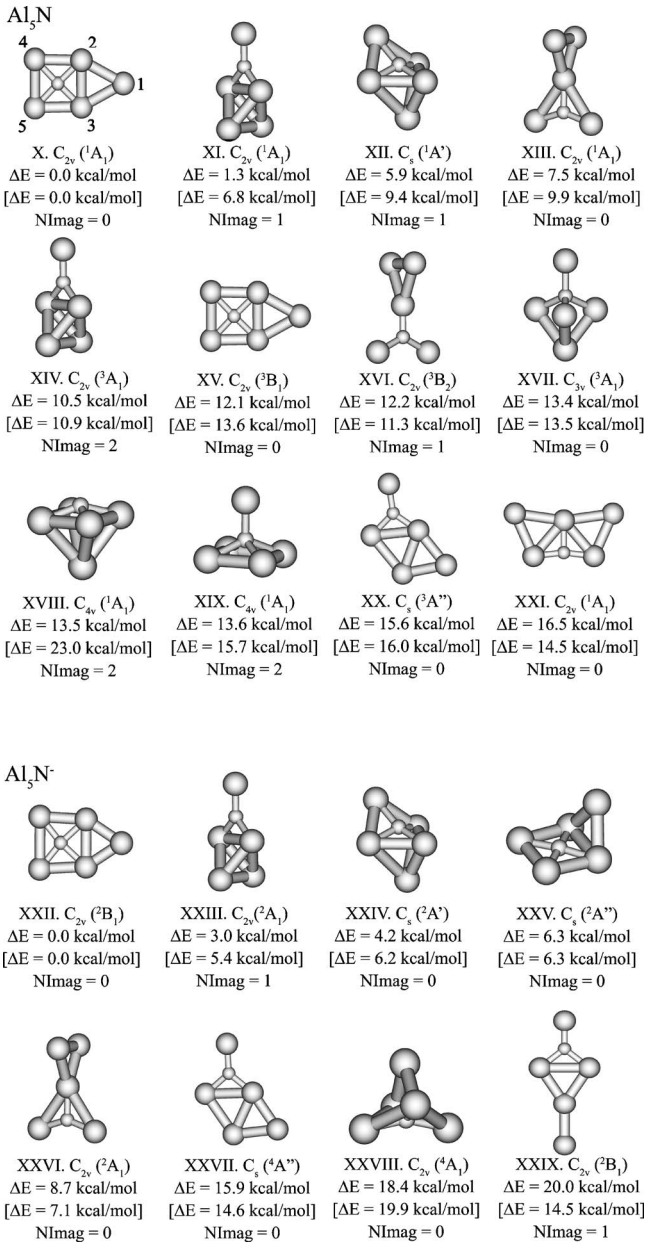

FIG. 6. The lowest isomers for Al_5N and Al_5N^-. Relative energies are presented at CCSD(T)/6-311+G(2*df*)//B3LYP/6-311+G* and at B3LYP/6-311+G* in brackets. N_{imag} is the number of imaginary frequencies calculated at B3LYP/6-311+G*.

instead of C_{2v}. Its relative energy is 5.4 kcal/mol at B3LYP/6-311+G* and 3.0 kcal/mol at CCSD(T)/6-311+G(2*df*)//B3LYP/6-311+G*. Geometry optimization at the CCSD(T)/6-311+G* level of theory revealed that $C_s(^2A')$ structure collapsed into the $C_{2v}(^2A_1)$ structure XXIII. The structure XXIII is 2.6 kcal/mol [CCSD(T)/6-311+G(2*df*)//CCSD(T)/6-311+G*] higher in energy than the global minimum. The third lowest energy structure XXIV $C_s(^2A')$ lies 6.2 kcal/mol at B3LYP/6-311+G*, 4.2 kcal/mol at CCSD(T)/6-311+G(2*df*)//B3LYP/6-311+G*, and 4.0 kcal/mol at CCSD(T)/6-311+G(2*df*)//CCSD(T)/6-311+G* higher in energy than the global minimum. In addition, two more structures XXV and XXVI were found to be about 6–8 kcal/mol [CCSD(T)/6-311+G(2*df*)//CCSD(T)/6-311+G*] above the global minimum. Other structures identified in our calculations, within 20 kcal/mol above the global minimum, are also shown in Fig. 6.

VI. COMPARISON OF CALCULATED VDEs WITH EXPERIMENT

A. Al_3N^-

The *ab initio* VDEs calculated at the TD-B3LYP/6-311+G(2*df*), ROVGF/6-311+G(2*df*), and CCSD(T)/6-311+G(2*df*) levels for Al_3N^- are compared with the experimental data in Table V, and good agreement is obtained among the different levels of theory and between the theory and experiment.

The global minimum of Al_3N^- was found to be the planar structure II (C_{2v},$^2B_2$) with the valence electronic configuration $1a_1^2 1b_2^2 2a_1^2 1b_1^2 3a_1^2 2b_2^2 4a_1^2 3b_2^1$. As given in Table V, our calculated VDE for removal of an electron from the HOMO of the global minimum is 1.06 eV at the UCCSD(T)/6-311+G(2*df*) level of theory, 1.16 eV at the UOVGF/6-311+G(2*df*) level of theory, and 1.15 eV at the TD-B3LYP/6-311+G(2*df*) level of theory. The pole strength (UOVGF) was found to be 0.90, indicating that the detachment channel can be primarily described by a one-electron detachment process. The calculated first VDE for the structure II (C_{2v},$^2B_2$) is in excellent agreement with the measured VDE of 1.19±0.04 eV for this feature (Table V). The $3b_2$-HOMO of Al_3N^- is a bonding orbital within the triangular wing Al–Al–Al in the global minimum structure (Fig. 7). Detachment of the electron from this orbital results in a significant geometry relaxation from C_{2v} in the anion to D_{3h} in the neutral. The large geometry change is consistent with the broad PES bandwidth observed for this transition (Fig. 1). The calculated adiabatic electron detachment energy (ADE) is 0.73 eV [CCSD(T)6-311+G(2*df*)//CCSD(T)/6-311+G*+ZPE//CCSD(T)/6-311+G*], in good agreement with the experimental threshold (~0.7 eV) for the X band. Because of the large geometry changes and the lack of vibrational resolution, the ADE cannot be accurately determined from the experimental PES spectra.

Electron detachment from the doubly occupied MOs could result in either triplet or singlet final states at the C_{2v} global minimum structure. The two triplet $^3B_2(1a_1^2 1b_2^2 2a_1^2 1b_1^2 3a_1^2 2b_2^2 4a_1^1 3b_2^1)$ and $^3A_1(1a_1^2 1b_2^2 2a_1^2 1b_1^2 3a_1^2 2b_2^1 4a_1^2 3b_2^1)$ states are assigned to the sharp features A and B, respectively (Table V), and the corresponding singlet $^1B_2(1a_1^2 1b_2^2 2a_1^2 1b_1^2 3a_1^2 2b_2^2 4a_1^1 3b_2^1)$ and $^1A_1(1a_1^2 1b_2^2 2a_1^2 1b_1^2 3a_1^2 2b_2^1 4a_1^2 3b_2^1)$ states are assigned to the relatively weak features C and D (Table V). The $4a_1$ and $2b_2$ MOs are essentially nonbonding (Fig. 7), consistent with the relatively sharp spectral features observed for bands A, B, C, and D. Finally, the broad feature E most probably corresponds to several transitions involving the two triplet $^3B_2(1a_1^2 1b_2^2 2a_1^2 1b_1^2 3a_1^1 2b_2^2 4a_1^2 3b_2^1)$ and $^3A_2(1a_1^2 1b_2^2 2a_1^2 1b_1^1 3a_1^2 2b_2^2 4a_1^2 3b_2^1)$ states (Table V). The $3a_1$ and $1b_1$ orbitals are strongly bonding MOs (Fig. 7), consistent with the broad E band.

TABLE V. Comparison of the experimental VDEs to calculated VDEs for structure II of the Al_3N^- anion.

Feature	VDE (Expt.) (eV)	Final state and electronic configuration	VDE (Theor.) (eV)		
			TD-B3LYP[a]	OVGF[a,b]	ΔCCSD(T)[a]
X	1.19 (4)	$^1A_1$, $1b_1^2 3a_1^2 2b_2^2 4a_1^2 3b_2^0$	1.15	1.16 (0.90)[a]	1.06
A	2.78 (3)	$^3B_2$, $1b_1^2 3a_1^2 2b_2^2 4a_1^1 3b_2^1$	2.78	2.92 (0.85)	2.71
B	3.06 (3)	$^3A_1$, $1b_1^2 3a_1^2 2b_2^1 4a_1^2 3b_2^1$	2.99	3.37 (0.85)[a]	3.15
C	3.39 (4)	$^1B_2$, $1b_1^2 3a_1^2 2b_2^2 4a_1^1 3b_2^1$	3.33		
D	3.69 (4)	$^1A_1$, $1b_1^2 3a_1^2 2b_2^1 4a_1^2 3b_2^1$	3.33		
E	5.20 (5)	$^3B_2$, $1b_1^2 3a_1^1 2b_2^2 4a_1^2 3b_2^1$	4.39	4.71 (0.79)[a]	
		$^3A_2$, $1b_1^1 3a_1^2 2b_2^2 4a_1^2 3b_2^1$	4.88	5.45 (0.90)[a]	

[a]6-311+G(2*df*) basis set.
[b]Values in parentheses represent the pole strength.

B. Al_4N^-

The calculated VDEs for the global minimum structure VII, as well as for the low-lying isomer VIII of Al_4N^-, are compared with the experimental data in Table VI. The calculated VDEs from the $1b_{2g}$ HOMO of the planar square D_{4h} structure VII at three levels of theory are 2.16 eV [TD-B3LYP/6-311+G(2*df*)], 2.26 eV [ROVGF/6-311+G(2*df*)], and 2.29 eV [CCSD(T)/6-311+G(2*df*)], agreeing very well with the experimental value of 2.32±0.03 eV (Table VI). The calculated adiabatic electron detachment energy (ADE) is 2.28 eV [CCSD(T)/6-311+G(2*df*)//CCSD(T)/6-311+ G* + ZPE//CCSD(T)/6-311+G*], in good agreement with the experimental value of 2.29 eV.[4]

The broadband (A and B) in the experimental spectra (Fig. 2) are due to detachment from HOMO-1 ($2e_u$) and HOMO-2 ($1b_{1g}$) (Table VI), which are very close to each other, resulting in the overlap of the two detachment bands. Because the order of the ^2E_u and $^2B_{1g}$ states is different at TD-B3LYP and OVGF, we cannot be sure with certainty which spectroscopic state is actually lower in energy. The next rather weak feature C could be assigned to detachment from HOMO-3 ($2a_{1g}$). According to our calculations there should be one detachment channel from HOMO-4 ($1a_{2u}$) around 6 eV (Table VI), which may be underestimated because no major detachment band was observed in the higher binding energy side. Overall, the calculated VDEs from the planar D_{4h} global minimum are in good agreement with the experiment, in particular, for the first three detachment channels.

The weak features, observed in the low energy part (<2.3 eV) of the spectrum and in between the intense peaks X and A (Fig. 2), cannot be explained by the global minimum D_{4h} structure and they should belong to either alternative isomers or to impurities. Nayak *et al.*[4] explained these small features by contributions from a triplet isomer. According to our calculations there are two lowest isomers: a triplet $C_{2v}(^3B_1)$ structure VIII [19.8 kcal/mol higher at CCSD(T)/6-311+G(2*df*)//B3LYP/6-311+G*] and singlet a C_s structure IX [21.8 kcal/mol higher at CCSD(T)/6-311+G(2*df*)//B3LYP/6-311+G*] (Fig. 5). Indeed the triplet $C_{2v}(^3B_1)$ structure VIII gives calculated VDEs, which fall in the right energy ranges for the weak features in the PES spectra of Al_4N^- (Table VI). Our result agrees with the previous assignment by Nayak *et al.*,[4] whose DFT calculations suggest that the triplet isomer is 0.97 eV (22.3 kcal/mol) above the D_{4h} ground state. It is very surprising that such a high energy isomer can be populated at all in the experiment. The explanation suggested by Nayak *et al.* that such a high energy isomer is "spin protected" seems reasonable, i.e., the triplet isomer once formed is prevented from being relaxed to the D_{4h} ground state because it is spin forbidden. Although this is unusual, we have increasingly observed in several cluster system population of high energy triplet isomers, for example, in B_7^- and B_{13}^-.[46,47]

C. Al_5N^-

We computed the VDEs from the three low-lying isomers for Al_5N^- and compared them with the experimental data in Tables VII–IX. Clearly, at least two isomers are needed to interpret the observed spectra of Al_5N^-. The OVGF and TD-DFT methods give a similar first VDE for all three isomers and cannot be used to distinguish them. However, our most accurate ΔCCST(T) method gives a first VDE of 2.01 eV for structure XXII, which is in good agreement with that of feature x (2.01 eV), whereas the first VDE for structure XXIII from ΔCCST(T) is 1.83 eV in very good agreement with that of feature X (1.89 eV), suggesting that the observed first two detachment bands come from two different isomers of Al_5N^-. The fact that the two features have similar intensities suggests that the two isomers are most likely degenerate, consistent with the close energies of the two isomers (Fig. 6).

The calculated second VDE from ΔCCST(T) for the planar C_{2v} structure XXII of Al_5N^- is 2.63 eV, in good agreement with that of band B (2.66 eV). The second ΔCCST(T) VDE for the C_{2v} structure XXIII is 2.23 eV, in excellent agreement with that of band A (2.29 eV). The next ΔCCST(T) detachment channel for both isomers is at much higher energies, thus preventing us from making more definitive assignments for the higher binding energies features. However, our TD-DFT data suggest that each of the higher binding energy feature may contain contributions from both isomers. We also computed the VDEs for isomer XXIV (Table IX), which seem to be all similar to those of the planar isomer XXII. Since this isomer is higher in energy, we suspect that it may not be significantly populated. Its minor contribution to the observed spectra is likely to be obscured.

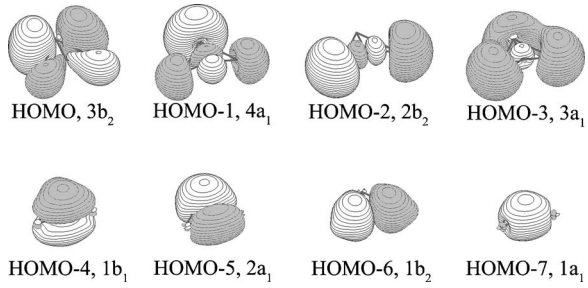

FIG. 7. Valence molecular orbitals for the structure II of Al_3N^- (UHF/6-311+G*).

Al_5N^- is a rare case, where two or more isomers are nearly degenerate and seem to be equally populated experimentally. The two isomers of Al_5N^- are very different, one planar (2D) (structure XXII) and the other 3D (structure XXIII). Al_3N^-, Al_3N, Al_4N^-, and Al_4N are all overwhelmingly stable as 2D structures. However, the 2D and 3D structures for Al_5N^- are nearly degenerate, signifying the onset of 2D to 3D transitions.

VII. CHEMICAL BONDING ANALYSES

A. Al_3N^- and Al_3N

The peculiar T shape for Al_3N^- can be understood on the basis of MO analysis, as shown in Fig. 7. The four lowest valence MOs (HOMO-7, HOMO-6, HOMO-5, and HOMO-4) are primarily formed from $2s$ (HOMO-7), $2p_x$ (HOMO-4), $2p_y$ (HOMO-6), and $2p_z$ (HOMO-5) atomic orbitals (AOs) of N. The next three MOs (HOMO-1, HOMO-2, and HOMO-3) corresponding to three lone pairs are formed primarily by $3s$ AOs of Al. When only these MOs are occupied as that in Al_3N, then the resulting structure is a perfect triangle with N being at the center and formal charge distribution is close to ionic $[(Al^+)_3(N^{3-})]$, i.e., Al is acting as a valence +1 atom. Indeed, our calculated natural bond orbital (NBO) effective charges $q(N)=-2.46|e|$ and $q(Al)=+0.82|e|$ (B3LYP/6-311+G*) support this simple ionic picture. The central N atom has already a full octet of valence electrons and it should not form any additional bonds. Thus one would expect that the Al_3N^- anion may not be an electronically stable species. That is indeed the case for NH_3, which does not bind an access electron.[48] However, the Al_3N^- anion is quite electronically stable with a VDE of 1.19 ± 0.04 eV. The stability of the Al_3N^- anion comes from the extra electron occupying $3b_2$-HOMO, which is a pure ligand (Al–Al) bonding orbital (Fig. 7). Calculated NBO effective charges $q(N)=-2.32|e|$, $q(Al_a)=+0.20|e|$, and $q(Al_e)=+0.56|e|$ (B3LYP/6-311+G*) support this description. The bonding character of the $3b_2$-HOMO is responsible for the electronic stability of this anion and for its T shape. The lower symmetry of Al_3N^- can also be understood as a Jahn-Teller distortion of the initial D_{3h} structure of Al_3N when an additional electron occupies its double degenerate LUMO ($3e'$).

B. Al_4N^- and Al_4N

The planar square structure of Al_4N^- can also be understood on the basis of the MO analysis, as shown in Fig. 8. The four lowest valence MOs (HOMO-6, HOMO-5, HOMO-5′, and HOMO-4) are again primarily formed from $2s$ (HOMO-6), $2p_x$ (HOMO-5′), $2p_y$ (HOMO-5), and $2p_z$ (HOMO-4) AOs of N. The next four MOs (HOMO-1, HOMO-2, HOMO-2′, and HOMO-3) corresponding to four lone pairs are formed primarily by $3s$ AOs of aluminum. When only these MOs are occupied as in Al_4N^+, the resulting structure is a tetrahedron with N being at the center and a formal charge distribution close to ionic, similar to the isoelectronic Al_4C molecule.[41,44] The tetrahedral Al_4C molecule has the following electron configuration $1a^2_1 1t^6_2 2a^2_1 2t^6_2 1e^0$. When one or two electrons occupy one of the doubly degenerate $1e$-LUMO, the resulting anions Al_4C^- and Al_4C^{2-} undergo Jahn-Teller distortion toward the planar D_{4h} structure.[41,45] Similarly, occupation of $1e$-LUMO in the tetrahedral Al_4N^+ should result in the geometric distortion towards D_{4h} structure in Al_4N and Al_4N^-. In Al_4N^+ the central atom N has a full octet and formally the hyperstoichiometric molecules Al_4N and Al_4N^- should not be stable. However, the ligand-ligand bonding HOMO in Al_4N and Al_4N^- is responsible for the electron and geometric stability

TABLE VI. Comparison of the experimental VDEs to calculated VDEs for Al_4N^-.

Feature	VDE (Expt.) (eV)	Final state and electronic configuration	VDE (Theor.) (eV) TD-B3LYP[a]	OVGF[a,b]	ΔCCSD(T)[a]
		Structure VII			
X	2.32 (3)	$^2B_{2g}$, $1a^2_{2u}2a^2_{1g}1b^2_{1g}2e^4_u1b^1_{2g}$	2.16	2.26 (0.87)	2.29
A	3.41 (2)	^2E_u, $1a^2_{2u}2a^2_{1g}1b^2_{1g}2e^3_u1b^2_{2g}$	3.38	3.63 (0.84)	3.52
B	3.74 (5)	$^2B_{1g}$, $1a^2_{2u}2a^2_{1g}1b^1_{1g}2e^4_u1b^2_{2g}$	3.47	3.56 (0.85)	3.53
C	5.40 (5)	$^2A_{1g}$, $1a^2_{2u}2a^1_{1g}1b^2_{1g}2e^4_u1b^2_{2g}$	5.21	5.79 (0.75)[c]	
		$^2A_{2u}$, $1a^1_{2u}2a^2_{1g}1b^2_{1g}2e^4_u1b^2_{2g}$	5.83		5.97
		Structure VIII			
	1.7–1.8	$^2A_1$, $1b^2_14a^2_12b^2_25a^2_16a^1_1$	1.63	1.84(0.88)	1.72
	1.9	$^2B_1$, $1b^2_14a^2_12b^2_25a^2_12b^1_1$	1.90	2.06(0.87)	2.03
	2.8	$^4B_1$, $1b^2_14a^2_12b^2_25a^1_16a^1_12b^1_1$	2.79	2.82(0.85)	2.82

[a]6-311+G(2*df*) basis set.
[b]Values in parentheses represent the pole strength.
[c]The pole strength is too low. This value is not reliable.

TABLE VII. Comparison of the experimental VDEs to calculated VDEs for the structure XXII of Al_5N^-.

Feature	VDE (Expt.) (eV)	Final state and electronic configuration	VDE (Theor.) (eV) TD-B3LYP[a]	UOVGF[a,b]	ΔCCSD(T)[a]
X	1.89 (4)				
x	2.01 (4)	$^1A_1$, $1b_1^2 4a_1^2 2b_2^2 3b_2^2 5a_1^2 6a_1^2 2b_1^2$	1.92	2.06 (0.88)	2.01
A	2.29 (3)				
B	2.66 (3)	$^3B_1$, $1b_1^2 4a_1^2 2b_2^2 3b_2^2 5a_1^2 6a_1^1 2b_1^1$	2.52	2.61 (0.86)	2.63
C	2.90 (3)	$^1B_1$, $1b_1^2 4a_1^2 2b_2^2 3b_2^2 5a_1^2 6a_1^1 2b_1^1$	2.77	[c]	[c]
D	3.27 (3)	$^3B_1$, $1b_1^2 4a_1^2 2b_2^2 3b_2^2 5a_1^1 6a_1^2 2b_1^1$	3.22	3.29 (0.84)	[c]
E	3.51 (3)	$^1B_1$, $1b_1^2 4a_1^2 2b_2^2 3b_2^2 5a_1^1 6a_1^2 2b_1^1$	3.47	[c]	[c]
F	3.87 (3)	$^1A_2$, $1b_1^2 4a_1^2 2b_2^2 3b_2^1 5a_1^2 6a_1^2 2b_1^1$	3.72	[c]	[c]
		$^3A_2$, $1b_1^2 4a_1^2 2b_2^2 3b_2^1 5a_1^2 6a_1^2 2b_1^1$	3.75	4.17 (0.84)	3.92
		$^3A_2$, $1b_1^2 4a_1^1 2b_2^1 3b_2^2 5a_1^2 6a_1^2 2b_1^1$	4.07	4.08 (0.83)	[c]
		$^1A_2$, $1b_1^2 4a_1^2 2b_2^1 3b_2^2 5a_1^2 6a_1^2 2b_1^1$	4.52	[c]	[c]
		$^3B_1$, $1b_1^2 4a_1^1 2b_2^2 3b_2^2 5a_1^2 6a_1^2 2b_1^1$	4.79	5.40 (0.78)[d]	[c]

[a]6-311+G(2*df*) basis set.
[b]Values in parentheses represent the pole strength.
[c]This value cannot be calculated at the this level of theory.
[d]The pole strength is too low. This value is not reliable.

of these species. Al_4N and Al_4N^- are analogs of the first experimentally discovered penta-atomic tetracoordinate planar carbon molecules, Al_4C^- and Al_4C^{2-}.[41–45]

C. Al_5N^- and Al_5N

The geometries of the structures X of Al_5N and XXII of Al_5N^- (Fig. 6) hint that they could be formally considered as Al^+ or Al coordinated to the edge of the planar Al_4N^- anionic structure VII (Fig. 5), respectively. Calculated NBO charges (B3LYP/6-311+G*) on the central nitrogen atom (−2.31 and $-2.33|e|$) are almost the same in Al_4N^- (VII), Al_5N (X), and Al_5N^- (XXII). The NBO charge on the apex Al atom in Al_5N is $+0.30|e|$, which is lower than ionic limit of $+1.0|e|$, but that is qualitatively consistent with the formal $[Al_4N]^-Al^+$ formulation, indicating the structural stability of the planar tetracoordinate $[Al_4N]^-$. In the anionic Al_5N^- cluster, a significant portion of the additional electron goes to the apex Al atom, which now has a NBO charge of $-0.25|e|$. The molecular orbital pictures for Al_5N and Al_5N^- (Fig. 9) are also consistent with the chemical bonding described above. One can see that molecular orbitals HOMO-1, HOMO-2, HOMO-3, HOMO-4, HOMO-5, HOMO-6, HOMO-8, HOMO-9, and HOMO-10 in Al_5N^- can be approximately correlated to the molecular orbitals HOMO, HOMO-2, HOMO-1, HOMO-2′, HOMO-3, HOMO-4, HOMO-5, HOMO-5′, and HOMO-6 in Al_4N^-, respectively. The HOMO and HOMO-7 are responsible for the π- and σ-covalent bondings between the apex Al atom and the Al_4N^- cluster.

The second lowest isomer of Al_5N (XI) could be formally considered as AlN^{2-} coordinated to the edge of the tetrahedral Al_4^{2+} dication. It was previously shown[38] that the Al_4^{2+} dication has a tetrahedral structure. Calculated NBO

TABLE VIII. Comparison of the experimental VDEs to calculated VDEs for the structure XXIII of Al_5N^-.

Feature	VDE (Expt.) (eV)	Final state and electronic configuration	VDE (Theor.) (eV) TD-B3LYP[a]	OVGF[a,b]	ΔCCSD(T)[a]
X	1.89 (4)	$^1A_1$, $2b_1^2 4a_1^2 2b_2^2 5a_1^2 6a_1^2 7a_1^0$	1.82	2.04 (0.86)	1.80
x	2.01 (4)				
A	2.29 (3)	$^3A_1$, $2b_1^2 4a_1^2 2b_2^2 5a_1^2 6a_1^1 7a_1^1$	2.04	2.17 (0.87)	2.23
B	2.66 (3)	$^1A_1$, $2b_1^2 4a_1^2 2b_2^2 5a_1^2 6a_1^1 7a_1^1$	2.64	[c]	[c]
C	2.90 (3)				
D	3.27 (3)	$^3A_1$, $2b_1^2 4a_1^2 2b_2^2 5a_1^1 6a_1^2 7a_1^1$	3.33	3.61 (0.85)	[c]
E	3.51 (3)	$^1A_1$, $2b_1^2 4a_1^2 2b_2^2 5a_1^1 6a_1^2 7a_1^1$	3.56	[c]	[c]
F	3.87 (3)	$^3B_2$, $2b_1^2 4a_1^2 2b_2^1 5a_1^2 6a_1^2 7a_1^1$	4.37	4.24 (0.79)[d]	4.16
		$^1B_2$, $2b_1^2 4a_1^2 2b_2^1 5a_1^2 6a_1^2 7a_1^1$	4.48	[c]	[c]
		$^3A_1$, $2b_1^2 4a_1^1 2b_2^2 5a_1^2 6a_1^2 7a_1^1$	4.40	5.17 (0.85)	[c]
		$^3B_1$, $2b_1^1 4a_1^2 2b_2^2 5a_1^2 6a_1^2 7a_1^1$	4.48	4.53 (0.82)	4.37
		$^1A_1$, $2b_1^2 4a_1^1 2b_2^2 5a_1^2 6a_1^2 7a_1^1$	4.84	[c]	[c]
		$^1B_1$, $2b_1^1 4a_1^2 2b_2^2 5a_1^2 6a_1^2 7a_1^1$	5.09	[c]	[c]

[a]6-311+G(2*df*) basis set.
[b]Values in parentheses represent the pole strength.
[c]This value cannot be calculated at the this level of theory.
[d]The pole strength is too low. This value is not reliable.

TABLE IX. Comparison of the experimental VDEs to calculated VDEs for the structure XXIV of Al_5N^-.

Feature	VDE (Expt.) (eV)	Final state and electronic configuration	VDE (Theor.) (eV) TD-B3LYP[a]	OVGF[a,b]	ΔCCSD(T)[a]
X	1.89 (4)				
x	2.01 (4)	$^1A'$, $4a'^25a'^26a'^22a''^27a'^23a''^28a'^0$	1.98	2.12 (0.88)	2.01
A	2.29 (3)				
B	2.66 (3)	$^3A''$, $4a'^25a'^26a'^22a''^27a'^23a''^18a'^1$	2.44	2.50 (0.87)	2.60
		$^1A''$, $4a'^25a'^26a'^22a''^27a'^23a''^18a'^1$	2.65		
C	2.90 (3)			[c]	[c]
D	3.27 (3)	$^3A'$, $4a'^25a'^26a'^22a''^27a'^13a''^28a'^1$	3.34	3.44 (0.86)	3.44
E	3.51 (3)	$^1A'$, $4a'^25a'^26a'^22a''^27a'^13a''^28a'^1$	3.56	[c]	[c]
F	3.87 (3)	$^3A'$, $4a'^25a'^26a'^12a''^27a'^23a''^28a'^1$	3.68	3.94 (0.85)	[c]
		$^3A''$, $4a'^25a'^26a'^22a''^17a'^23a''^28a'^1$	3.81	3.72 (0.86)	[c]
		$^1A''$, $4a'^25a'^26a'^22a''^17a'^23a''^28a'^1$	3.99	[c]	[c]
		$^3A'$, $4a'^25a'^16a'^22a''^27a'^23a''^28a'^1$	4.27	4.42 (0.84)	[c]
		$^1A'$, $4a'^25a'^16a'^22a''^27a'^23a''^28a'^1$	4.37	[c]	[c]
		$^1A'$, $4a'^14a'^26a'^22a''^27a'^23a''^28a'^1$	4.81	[c]	[c]

[a]6-311+G(2*df*) basis set.
[b]Values in parentheses represent the pole strength.
[c]This value cannot be calculated at the this level of theory.

charge (B3LYP/6-311+G*) on the AlN group is $-1.42|e|$ and that is qualitatively consistent with the formal $[Al_4]^{2+}(NAl)^{2-}$ formulation. According to our NBO analysis of Al_5N^- (XXIII), an additional electron in Al_5N^- goes to the Al_4 unit.

VIII. CONCLUSIONS

Well-resolved photoelectron spectra were obtained for three nitrogen-doped aluminum clusters Al_3N^-, Al_4N^-, and Al_5N^- at four photon energies (532, 355, 266, and 193 nm) and compared with theoretical calculations to elucidate their electronic structure and chemical bonding. Global minimum structures of Al_3N^-, Al_4N^-, and Al_5N^- were identified first by using gradient embedded genetic algorithm (B3LYP/3-21G) followed by B3LYP/6-311+G*, MP2/6-311+G*, and CCSD(T)/6-311+G* geometry and frequency calculations. By comparing the theoretical VDEs with the experimental data, we established that NAl_3 is D_{3h} and Al_3N^- has a T-shaped structure (II) $C_{2v}(^2B_2)$. The ground states of Al_4N and Al_4N^- are both square planar in agreement with previously reported results. For the Al_5N^- anion we found two quasidegenerate structures XXII (C_{2v}, $^2B_1$) and XXIII (C_{2v}, $^2A_1$), which are almost equally populated experimentally. We also computationally identified three other low energy structures: XXIV (C_s, $^2A'$), XXV (C_s, $^2A''$), and XXVI (C_{2v}, $^2A_1$), which lie with 6–8 kcal/mol above the ground state. The low-lying isomers of the neutral Al_5N cluster are found to be similar to those of its anion.

Chemical bonding analysis revealed that Al_3N can be described as an ionic cluster $(Al^+)_3(N^{3-})$. In the planar C_{2v} structure of Al_3N^-, an additional electron occupies the peripheral ligand-ligand bonding HOMO, resulting in the structural distortion to the T shape. Both Al_4N and Al_4N^- have

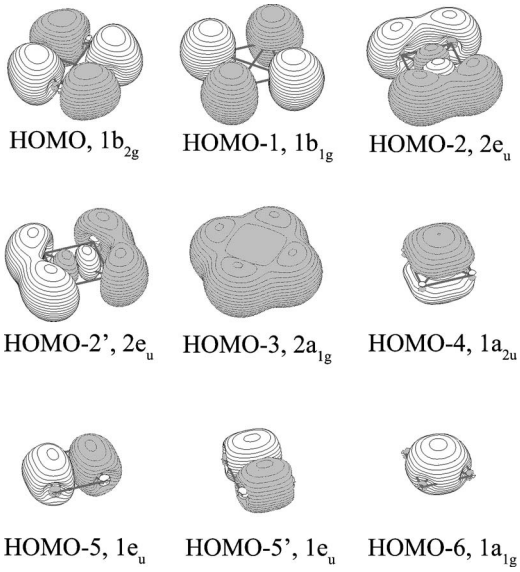

FIG. 8. Valence molecular orbitals for the structure VII of Al_4N^- (RHF/6-311+G*).

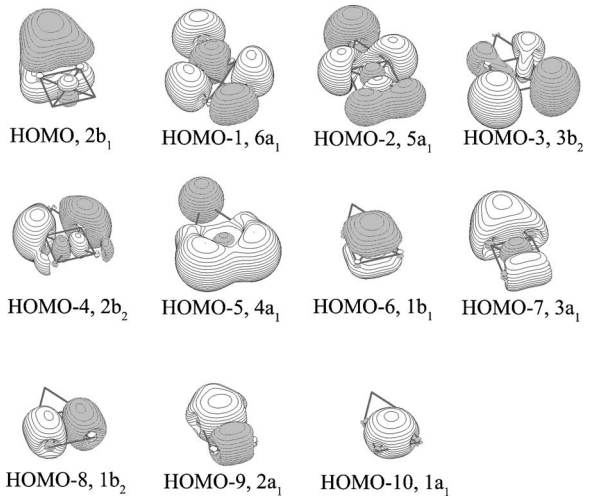

FIG. 9. Valence molecular orbitals for the structure XXII of Al_5N^- (UHF/6-311+G*).

planar structure with a central nitrogen atom. The planarity of this structure is due to the singly or doubly occupied $1b_{2g}$-HOMO, which is a peripheral four-center ligand-ligand bonding orbital, similar to the tetracoordinate planar carbon molecules, CAl_4^- and CAl_4^{2-}. Finally, for the Al_5N and Al_5N^- species, two nearly degenerate structures competing for the ground state, a planar one and a 3D one. The planar structure can be viewed as an Al coordinated to the planar Al_4N^-: $[Al_4N]^-Al^+$ or $[Al_4N]^-Al$, whereas the 3D structure can be viewed as an AlN unit interacting with a tetrahedral Al_4 motif: $[Al_4]^{2+}(NAl)^{2-}$ or $[Al_4]^+(NAl)^{2-}$.

ACKNOWLEDGMENTS

The theoretical work done at Utah State University was supported by The Petroleum Research Fund (ACS-PRF No. 43101-AC6), administered by the American Chemical Society and by the National Science Foundation (CHE-0404937). Computer time from the Center for High Performance Computing at Utah State University is gratefully acknowledged. The computational resource, the Uinta cluster supercomputer, was provided through the National Science Foundation under Grant No. CTS-0321170 with matching funds provided by Utah State University. The experimental work done at Washington State University was supported by the National Science Foundation (DMR-0503383) and was performed at the W. R. Wiley Environmental Molecular Sciences Laboratory, a national scientific user facility sponsored by DOE's Office of Biological and Environmental Research and located at Pacific Northwest National Laboratory, which is operated for DOE by Battelle.

[1] P. v. R. Schleyer and A. I. Boldyrev, J. Chem. Soc., Chem. Commun. **1991**, 1536.
[2] V. G. Zakrzewski, W. v. Niessen, A. I. Boldyrev, and P. v. R. Schleyer, Chem. Phys. **174**, 167 (1993).
[3] S. K. Nayak, S. N. Khana, and P. Jena, Phys. Rev. B **57**, 3787 (1998).
[4] S. K. Nayak, B. K. Rao, P. Jena, X. Li, and L. S. Wang, Chem. Lett. **301**, 379 (1999).
[5] B. H. Boo and Z. Liu, J. Phys. Chem. A **103**, 1250 (1999).
[6] L. Andrews, M. Zhou, G. V. Chertihin, W. D. Bare, and Y. Hannachi, J. Phys. A **104**, 1656 (2000).
[7] B. R. Leskiw, A. W. Castleman, Jr., C. Ashman, and S. N. Khanna, J. Chem. Phys. **114**, 1165 (2001).
[8] L. Ling, B. Song, and P.-L. Cao, J. Mol. Struct.: THEOCHEM **728**, 215 (2005).
[9] L. Gou and H.-S. Wu, Int. J. Quantum Chem. **106**, 1250 (2006).
[10] X. Li and L. S. Wang, Eur. Phys. J. D **34**, 9 (2005).
[11] G. Meloni, S. M. Sheehan, B. F. Parsons, and D. M. Neumark, J. Phys. Chem. A **110**, 3527 (2006).
[12] L. S. Wang, H. S. Cheng, and J. Fan, J. Chem. Phys. **102**, 9480 (1995).
[13] A. N. Alexandrova, A. I. Boldyrev, Y.-J. Fu, X.-B. Wang, and L. S. Wang, J. Chem. Phys. **121**, 5709 (2004).
[14] A. N. Alexandrova and A. I. Boldyrev, J. Chem. Theory Comput. **1**, 566 (2005).
[15] A. D. Becke, J. Chem. Phys. **98**, 5648 (1993).
[16] S. H. Vosko, L. Wilk, and M. Nusair, Can. J. Phys. **58**, 1200 (1980).
[17] C. Lee, W. Yang, and R. G. Parr, Phys. Rev. B **37**, 785 (1988).
[18] J. S. Binkley, J. A. Pople, and W. J. Hehre, J. Am. Chem. Soc. **102**, 939 (1980); M. S. Gordon, J. S. Binkley, J. A. Pople, W. J. Pietro, and W. J. Hehre, *ibid.* **104**, 2797 (1982); W. J. Pietro, M. M. Francl, W. J. Hehre, D. J. Defrees, J. A. Pople, and J. S. Binkley, *ibid.* **104**, 5039 (1982).
[19] M. Head-Gordon, J. A. Pople, and M. J. Frisch, Chem. Phys. Lett. **153**, 503 (1988).
[20] J. Cizek, Adv. Chem. Phys. **14**, 35 (1969).
[21] P. J. Knowles, C. Hampel, and H.-J. Werner, J. Chem. Phys. **99**, 5219 (1993).
[22] K. Raghavachari, G. W. Trucks, J. A. Pople, and M. Head-Gordon, Chem. Phys. Lett. **157**, 479 (1989).
[23] A. D. McLean and G. S. Chandler, J. Chem. Phys. **72**, 5639 (1980).
[24] T. Clark, J. Chandrasekhar, G. W. Spitznagel, and P. v. R. Schleyer, J. Comput. Chem. **4**, 294 (1983).
[25] M. J. Frisch, J. A. Pople, and J. S. Binkley, J. Chem. Phys. **80**, 3265 (1984).
[26] F. Bernardi, A. Bottini, J. J. W. McDougall, M. A. Robb, and H. B. Schlegel, Faraday Symp. Chem. Soc. **19**, 137 (1979).
[27] M. J. Frisch, I. N. Ragazos, M. A. Robb, and H. B. Schlegel, Chem. Phys. Lett. **189**, 524 (1992).
[28] L. Cederbaum, J. Phys. B **8**, 290 (1975).
[29] W. von Niessen, J. Shirmer, and L. S. Cederbaum, Comput. Phys. Rep. **1**, 57 (1984).
[30] V. G. Zakrzewski and W. von Niessen, J. Comput. Chem. **14**, 13 (1993).
[31] J. V. Ortiz, Int. J. Quantum Chem., Quantum Chem. Symp. **23**, 321 (1989); J. S. Lin and J. V. Ortiz, Chem. Phys. Lett. **171**, 197 (1990).
[32] V. G. Zakrzewski, J. V. Ortiz, J. A. Nichols, D. Heryadi, D. L. Yeager, and J. T. Golab, Int. J. Quantum Chem. **60**, 29 (1996).
[33] R. Bauernshmitt and R. Alrichs, Chem. Phys. Lett. **256**, 454 (1996).
[34] M. E. Casida, C. Jamorski, K. C. Casida, and D. R. Salahub, J. Chem. Phys. **108**, 4439 (1998).
[35] M. J. Frisch, G. M. Trucks, H. B. Schlegel *et al.*, GAUSSIAN 98, Revision A.7, Gaussian, Inc., Pittsburgh, PA, 1998.
[36] M. J. Frisch, G. M. Trucks, H. B. Schlegel *et al.*, GAUSSIAN 03, Revision A.1, Gaussian, Inc., Pittsburgh, PA, 2003.
[37] G. Schaftenaar, MOLDEN3.4, CAOS/CAMM Center, The Netherlands, 1998.
[38] A. I. Boldyrev and P. v. R. Schleyer, J. Am. Chem. Soc. **113**, 9045 (1991).
[39] J. Sun, W. C. Lu, H. Wang, Z.-S. Li, and C.-C. Sun, J. Phys. Chem. A **110**, 2729 (2006).
[40] A. I. Boldyrev, X. Li, and L. S. Wang, J. Phys. Chem. **104**, 5358 (2000).
[41] X. Li, L. W. Chen, L. S. Wang, A. I. Boldyrev, and J. Simons, J. Am. Chem. Soc. **121**, 6033 (1999).
[42] A. I. Boldyrev and J. Simons, J. Am. Chem. Soc. **120**, 7967 (1998).
[43] L. S. Wang, A. I. Boldyrev, X. Li, and J. Simons, J. Am. Chem. Soc. **122**, 7681 (2000).
[44] D. Yu. Zubarev and A. I. Boldyrev, J. Chem. Phys. **122**, 144322 (2005).
[45] X. Li, H.-F. Zhang, L. S. Wang, G. D. Geske, and A. I. Boldyrev, Angew. Chem., Int. Ed. **39**, 3630 (2000).
[46] A. N. Alexandrova, A. I. Boldyrev, H. J. Zhai, and L. S. Wang, J. Phys. Chem. A **108**, 3509 (2004).
[47] H. J. Zhai, B. Kiran, J. Li, and L. S. Wang, Nat. Mater. **2**, 827 (2003).
[48] H. W. Sarkas, S. T. Arnold, J. G. Eaton, G. H. Lee, and K. H. Bowen, J. Chem. Phys. **116**, 5731 (2002).